Production of multicharged atomic ions from laser-induced multiple ionization of small molecules

Ph. Hering and C. Cornaggia
CEA Saclay, Direction des Sciences de la Matière, Service des Photons, Atomes et Molécules, F-91191 Gif-sur-Yvette, France
(Received 14 July 1997; revised manuscript received 2 February 1998)

The production of C^{Z+}, N^{Z+}, and O^{Z+} multicharged atomic ions up to $Z=4$ is investigated using the laser-induced multiple ionization of small molecules in the gas phase in the 10^{15}–10^{16}-W/cm^2 laser intensity range. For molecules built with a single C, N, or O atom and hydrogen atoms such as CH_4, NH_3, and H_2O, the $Z=3$ and 4 ion yields are systematically weaker than for molecules built with equivalent atoms such as N_2, CO, O_2, CO_2, and N_2O using rigorously the same laser excitation conditions. In particular, the C^{4+}, N^{4+}, and O^{4+} ion production efficiency is more than one order of magnitude lower in the first case. In addition, no significant differences are found for the ion production efficiency between diatomic and linear triatomic molecular species built with the same atoms. This overall behavior remains the same at lower laser intensities in the 10^{14}–10^{15}-W/cm^2 range for lower atomic ions charge states. The experimental results are in good qualitative agreement with recent theoretical models of molecules in strong laser fields. In order to get quantitative agreement, the initial three-dimensional electronic configuration of each molecule has to be included in nonperturbative theories. [S1050-2947(98)01506-6]

PACS number(s): 33.80.Rv, 33.80.Eh, 42.50.Vk

I. INTRODUCTION

Multiple charged atomic ions can be produced using a wide variety of excitation mechanisms of atoms, molecules, and surfaces based mainly on electron impact, field ionization, laser-plasma interactions, and ion stripping in a thin foil. Many types of ion sources have been developed because of the large interest in fundamental research and industrial applications in astrophysics, fusion research, and radiation therapy. This paper deals with the production of multicharged atomic ions C^{Z+}, N^{Z+}, and O^{Z+} from different molecular targets using an intense femtosecond laser field in the 10^{15}–10^{16}-W/cm^2 laser intensity range. Since this study is aimed at the primary effects of molecular multiple ionization, the interaction takes place in the gas phase regime at very low operating pressures in the 10^{-9}-Torr range. No collective and plasma effects occur in the electron stripping processes and ion detection measurements.

Usually, the laser-induced multiple ionization of atoms and molecules is performed with picosecond and femtosecond laser systems operating in the optical domain for wavelengths from 193 to 1064 nm that depend on the laser-gain medium. The outer-shell electrons interact with the laser field and are ejected from the initial atom or molecule X following

$$X + \text{laser} \rightarrow X^{Z+} + Ze^- + \text{energy}. \tag{1}$$

In the atomic case, simple models based on barrier suppression ionization give the correct order of magnitude for the saturation laser intensity that is necessary to produce a X^{Z+} ion from a $X^{(Z-1)+}$ precursor ion [1,2]. However, below the saturation intensity, direct multiple ionization was observed for the production of He^{2+}, Ar^{2+}, Ar^{3+}, Xe^{2+}, and Xe^{3+} ions [2]. Recent detailed experimental and theoretical studies performed with helium have shown unambiguously that direct double ionization of helium dominates the He^{2+} ion yield at $\lambda=780$ nm, $\tau=160$ (pulse duration) fs in the 10^{14}–10^{15}-W/cm^2 intensity range [3,4].

For molecules, the X^{Z+} molecular ion is in general unstable for $Z>2$ and gives rise to atomic multicharged ions following

$$[ABC^{Z+}] \rightarrow A^{Z'+} + B^{Z''+} + C^{Z'''+} + \text{kinetic energy release}, \tag{2}$$

where $X^{Z+}=[ABC^{Z+}]$ represents the transient undetected molecular ion. The multiple ionization of the initial neutral molecule is more complicated than in the atomic case basically because of the multicenter nuclear field experienced by the valence electrons and the evolution of the nuclear structure in the course of the electronic emission. This problem has initiated much experimental work, especially for diatomic molecules, since the pioneering of Frasinski *et al.* [5]. At the beginning of the 1990s, it was found that the measured kinetic-energy releases were systematically weaker than the expected Coulomb repulsion energy ZZ'/R_e starting at the equilibrium internuclear distance R_e of the neutral molecule for a diatomic fragmentation $AB \rightarrow A^{Z+} + B^{Z'+}$ [6,7]. As a consequence, it was deduced that the Coulomb repulsion between the fragments begins at a critical internuclear distance R_c larger than R_e. In addition, the R_c distance was found to be quasi-independent of the charge states (Z,Z') of the repelling ions. Recent theoretical models developed for diatomic molecules and based on field ionization [8] and time-dependent nonperturbative quantum calculations [9–11] are in good agreement with the experimental findings. Although these two approaches are very different, the main conclusions of these models are that the laser-molecule coupling strength and, as a consequence, the multiple ionization are much more efficient at internuclear distances larger than the R_e. According to Seideman *et al.* and Yu and co-workers, the nonadiabatic localization of the electronic wave function in the rising well of the two-center po-

tential [9,10] and the phenomenon of charge-enhanced ionization [10,11] are crucial elements of the models.

The main purpose of this paper concerns the choice of the molecular targets to produce efficiently C^{Z+}, N^{Z+}, and O^{Z+} ions from simple diatomic and polyatomic gases available quite easily without any specific chemical preparation. For each atomic species, a set of molecules was studied using exactly the same laser intensity and ion detection conditions. The aim of our measurements is to determine the role of the atomic environment within the molecule for an efficient multiple ionization. For instance, in the case of atomic nitrogen, the N^{Z+} ion yields coming, respectively, from NH_3, N_2, and N_2O will be compared. Since the electronic and nuclear structures of these molecules are different, the laser-molecule coupling is expected to be molecular dependent even in the strong laser field regime. For NH_3 the electronic distribution lies closer to the N atom than for N_2 and N_2O. As a consequence, the intramolecular charge-transfer processes between, respectively, the N^{Z+} and H^+ ions and the N^{Z+} and O^{Z+} ions will be different. In addition, the departure of the light protons of NH_3 can inhibit the electronic localization along the N-H axes. In this case, the multiple ionization would be less efficient than in N_2 and closer to the multiple ionization of a bare N atom.

The second important point concerns the efficiency of the laser-molecule coupling and the associated multiple ionization as a function of the number of bonds, for instance, one bond in N_2 and CO and two bonds in N_2O and CO_2. To our knowledge, theoretical developments were detailed for diatomic molecules, which represent a two-well nuclear field problem in the presence of the intense laser field. In the triatomic case, the concept of nonadiabatic localization of the electronic wave function is more difficult to deal with. In particular, a comparison with the diatomic case will tell us if the localization concerns only two wells or involves the interplay of three wells. In the first case, we expect ions yields with the same order of magnitude for di- and triatoms, while in the second case the concerted electron transfer between the three wells might enhance the multielectron ionization.

The paper is organized as follows. Section II describes the experimental setup (Sec. II A is for the laser system and Sec. II B is for the time-of-flight detection) and the operating conditions for the data presented in this work (Sec. II C). Section II presents the experimental result for the N^{Z+} (Sec. III A), C^{Z+} (Sec. III B), and O^{Z+} (Sec. III C) ion production efficiencies. Section IV is devoted to the discussion of the experimental results and comparisons with field ionization models (Sec. IV A) and more sophisticated time-dependent nonperturbative theories (Sec. IV B).

II. EXPERIMENTAL SETUP

A. The laser system

The femtosecond laser system is a commercial kilohertz laser chain based on a titanium-sapphire gain medium. A self-mode-locked oscillator (Mira from COHERENT modified by MC2), pumped by an Ar^+ cw laser, delivers pulses with a wavelength spectrum centered at $\lambda=800$ nm and pulse duration $\tau=27$ fs. The amplification (B. M. Industries) is performed using the chirp pulse amplification technique: The laser pulse from the oscillator is stretched to a pulse duration

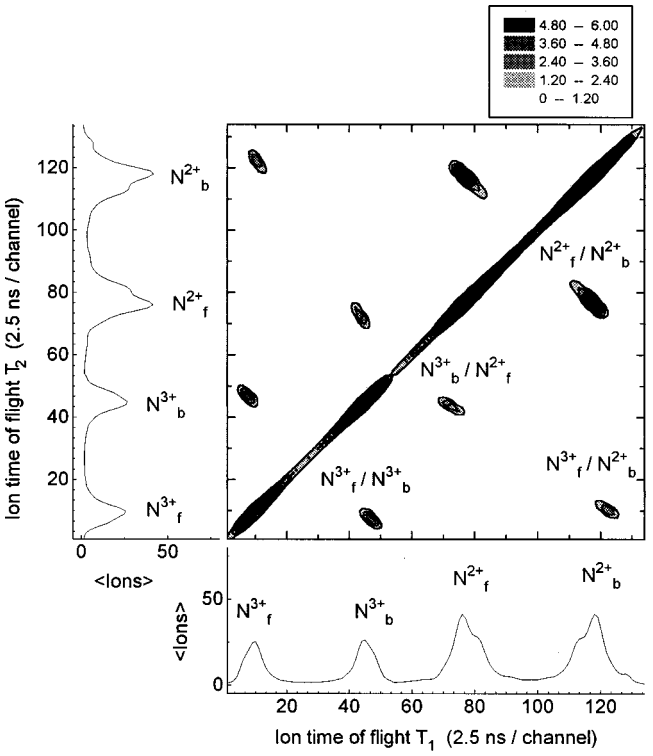

FIG. 1. Covariance map of N_2 recorded at $\lambda=800$ nm, $I=1.4\times10^{16}$ W/cm^2, and $p(N_2)=1.5\times10^{-9}$ Torr with the laser polarization direction parallel to detection axis. The covariance coefficient $C^{(2)}(T_1,T_2)$ is represented using a five-level gray scale as a function of the T_1 (horizontal axis) and T_2 (vertical axis) ion times of flight. The fragmentation channels are $N^{2+}+N^{2+}+24$ eV, $N^{3+}+N^{2+}+36$ eV, and $N^{3+}+N^{3+}+56$ eV. The relative error on the energy measurements is $\Delta E/E=\pm5\%$.

$\tau=300$ ps, then the amplification takes place in a regenerative amplifier pumped by a kilohertz Nd^{3+}:YLF laser, and finally the pulse duration is recompressed to typically $\tau=40$ fs using a two-grating compressor. The laser pulse duration is measured using standard second-order autocorrelation techniques. The laser system output at 1 kHz is typically 750 μJ at $\lambda=800$ nm.

B. The time-of-flight ion detection

The laser-molecule interaction takes place in a high vacuum chamber with a residual pressure of 3×10^{-10} Torr. The ions are detected by a Wiley-McLaren short time-of-flight drift tube (100 mm), specially designed for the multifragmentation studies of multicharged molecules [12]. Briefly, the spectrometer is operated so that the time of flight exhibits a linear dependence of the ion initial momentum. The fragmentation channels are identified using statistical correlations techniques [13]. For this purpose, the spectrometer is equipped with 40-mm-diam and 90% high transmission grids in order to collect all the ions coming from the molecular multifragmentation. Figure 1 represents the covariance map recorded with the N_2 molecule for the identification of the $N^{Z+}+N^{Z'+}$ $(Z,Z'=2,3)$ channels. The ion collection electric field is 180 V/cm and the laser polarization direction is parallel to the spectrometer axis. Since the molecule is aligned along the laser electric field, the N^{Z+} ions

are ejected along the spectrometer axis and present a highly symmetric double-peak structure coming from the backward (N_b^{Z+}) and the forward (N_f^{Z+}) initial emission directions relative to the detector position.

This study reports the total A^{Z+} ion yield whatever the parent ionization channel $ABC+\text{laser}\rightarrow A^{Z+}+B^{Z'+}+C^{Z''+}$. As a consequence, no effort is made for the identification of the associated $B^{Z'+}, C^{Z''+}$ ions. Moreover, the A^{Z+} double-peak structure due to the initial momentum might complicate in some cases the time-of-flight spectrum. In order to avoid this problem, the laser polarization direction is set perpendicular to the spectrometer axis. Then the ion peaks present a single-peak structure with a width that is proportional to the width of the initial momenta $P_\perp$ distribution, where $P_\perp$ is the momentum component perpendicular to the laser electric field [14]

The main difference with respect to the ion-ion correlation experiments is the use of a rectangular slit (300 μm$\times$40 mm) instead of a grid for the output electrode of the ion collection chamber. In the case of a grid, the entire ionization volume is ''seen'' by the ion detector and the ion yield reflects the Gaussian distribution of the laser intensity $I(r,z)$ within the focal volume [15]

$$I(r,z)=I_{\max}[r_0/r(z)]^2\exp\{-2[r/r(z)]^2\}, \qquad (3)$$

where $r(z)^2=r_0^2[1+(z/z_0)^2]$. In the above equation, z and r are the cylindrical coordinates with z along the laser beam propagation, $I_{\max}$ is the maximum laser intensity, r_0 is the beam radius at the best focus, and z_0 is the Rayleigh range. For instance, for $I_{\max}=10^{16}$ W/cm^2, the volume for laser intensities between 10^{13} and 2×10^{15} W/cm^2 is 2400 times the volume for laser intensities between 2×10^{15} W/cm^2 and $I_{\max}=10^{16}$ W/cm^2. In order to avoid the too large Lorentzian distribution of laser intensities along the propagation axis, the width $l=300$ μm is chosen to be around 4 times the Rayleigh range $z_0=70$ μm for our focal length $F=75$ mm. In this case, the laser intensity for the collected ions varies from $I_{\max}$ to $I_{\max}/5$ on axis at $r=0$. The transverse dimension of the slit is $L=40$ mm in order to collect all the ions ejected in a direction perpendicular to the spectrometer axis and to the laser propagation direction (i.e., parallel to the laser polarization direction). For all the data presented in this paper, the collection electric field is 500 V/cm, which is sufficient to avoid energetic ions losses.

Figure 2 represents three time-of-flight (TOF) spectra recorded, respectively, with grids [Fig. 2(a)] and with the slit [Figs. 2(b) and 2(b)] for the N_2O molecule. In Figs. 2(a) and 2(b) the laser electric field is parallel to the spectrometer axis and in Fig. 2(c) these two directions are perpendicular. These three spectra were obtained with the same laser intensity and N_2O pressure. In Fig. 2(b) the ion yield is less than in Fig. 2(a) because of the slit discrimination against the focal volume extension. In particular, the N_2O^+ molecular ion peak is 8 times weaker because the N_2O^+ ions are created and not subsequently ionized in the periphery of the focal volume. One interesting feature is that the ion production from the background H_2O molecule (H^+ and H_2O^+) is also noticeably weaker for the same reasons. The ratio between the A^{3+} and A^{2+} (A=N,O) ion numbers is larger because the slit discrimination favors the higher intensities. Finally, the comparison between Figs. 2(b) and 2(c) shows that the ion loss remains very small in the perpendicular configuration. Moreover, the spectrum of Fig. 2(c) is simpler for the analysis of the multicharged atomic ion yields.

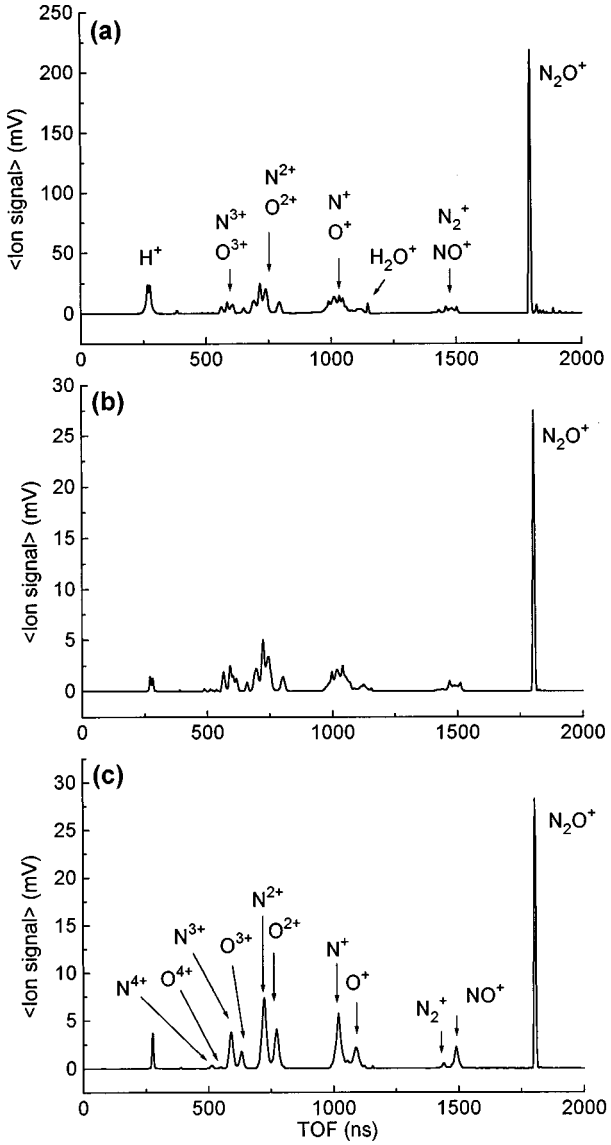

FIG. 2. Time-of-flight spectra of N_2O recorded at $\lambda=800$ nm, $I=5\times10^{15}$ W/cm^2, and $p(N_2O)=10^{-8}$ Torr with (a) 40-mm circular aperture high transmission grids and laser polarization direction parallel to the detection axis, (b) the 300 μm$\times$40 mm rectangular aperture slit and laser polarization direction parallel to the detection axis, and (c) the 300 μm$\times$40 mm rectangular aperture slit and laser polarization direction perpendicular to the detection axis.

C. Conclusions and operating conditions

All the time-of-flight spectra presented in Sec. III have been recorded with the same laser excitation conditions ($\lambda=800$ nm and $I=6\times10^{15}$ W/cm^2) and the same collection electric field $F_c=500$ V/cm of the ion spectrometer equipped with the 0.3$\times$40-mm^2 slit. Concerning the laser pulse duration in the high vacuum chamber, no direct measurements were made because of the divergent beam profile after the focal spot. Systematic comparisons with the multicharged

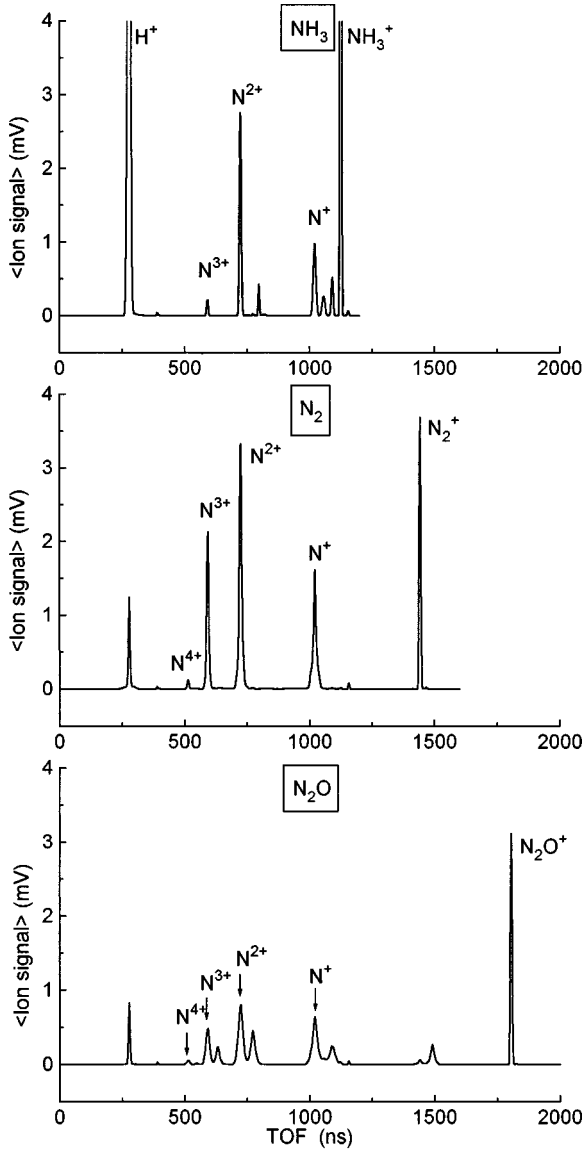

FIG. 3. Time-of-flight spectra of NH_3, N_2, and N_2O recorded at $\lambda=800$ nm, $I=6\times10^{15}$ W/cm^2, and $p=10^{-9}$ Torr.

atomic ion yields (for N_2 and CO_2) obtained with a 130-fs titanium:sapphire laser were performed as a function of the laser initial energy while the spectrometer and optical components were rigorously identical. Our main conclusion is that the laser pulse duration is 50 ± 10 fs at the best focus with an optimization of the compressor to compensate for the positive group velocity dispersion introduced by the optical elements. Moreover, the focusing aperture is $F/10$, so that the temporal broadening due to the lens curvatures remains very small. Finally, no corrections were made for the electron current from the microchannel plate detector as a function of the charge state of the detected ion since we compare the same A^{Z+} ion production from different molecules. For each A^{Z+} species, the total ion number is proportional to the total area of the time-of-flight ion peak. In the comparisons presented in the next section, they are expressed in practical units (mV×ns) since the microchannel plate signal is measured in mV through a 50-Ω load resistor. The spectra are presented for a reference pressure of $p=10^{-9}$ Torr, which is the typical operating pressure for the ion detection. In this

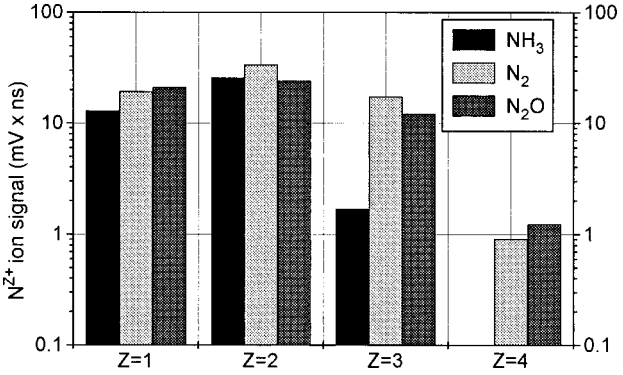

FIG. 4. Production of N^{Z+} for $Z=1-4$ from NH_3, N_2, and N_2O gases at $\lambda=800$ nm, $I=6\times10^{15}$ W/cm^2, and $p=10^{-9}$ Torr.

case, the multiplicative corrective factors furnished by the supplier of the ionization gauge (ALCATEL) are applied to the ion signal for each gas introduced in the vacuum chamber.

III. EXPERIMENTAL RESULTS

A. Molecules with N atoms

Figure 3 represents the TOF spectra recorded with NH_3, N_2, and N_2O molecules. The NH_3^+ ion peak is 4 and 3 times larger than, respectively, the N_2^+ and N_2O^+ ion peaks. The first reason for this observation is that the 10.15-eV ionization potential of NH_3 is lower than, respectively, the 15.58-eV and 12.89-eV ionization potentials of N_2 and N_2O. The second reason is related to the total number of multicharged ions. Indeed, the main feature of Fig. 4 shows that NH_3 gives definitively fewer N^{Z+} multicharged atomic ions than N_2 and N_2O. Since the multiple ionization is less efficient for this molecule, the precursor ion NH_3^+ remains larger than expected from a more efficient subsequent ionization. In addition, the NH^+ and NH_2^+ ion peaks lying in the TOF spectrum between the N^+ and NH_3^+ ion peaks represent, respectively, 3% and 2% the NH_3^+ ion number. This suggests that the observed N^{Z+} ions come mainly from the multiple ionization and multiple fragmentation of NH_3^+ precursor ions.

In the case of N_2 and N_2O, the N_2^+ ion peak is 1.2 times larger than the N_2O^+ ion peak, although the N_2 ionization potential is larger than the N_2O ionization potentials. This observation is due to the additional $N^+ + NO^+$ and $N_2^+ + O^+$ channels [16] in the N_2O case that decrease the N_2O^+ detected ion number. Finally, the widths of the N^{Z+} ion peaks increase from NH_3 to N_2O. In the NH_3 multifragmentation, the kinetic energy releases are mainly taken by the light protons, while in the N_2 case they are shared by the N^{Z+} ion. In the N_2O case, the three-body Coulomb repulsion produces kinetic energy releases higher than in the N_2 case. The unlabeled companion O^{Z+} ion peaks in the TOF spectrum of N_2O are 2 times weaker than the N^{Z+} ion peaks for the simple reason that N_2O has one O atom and two N atoms. For the three molecules, the N^{Z+} ion yields are reported in Fig. 4. The N^+ and N^{2+} ion productions are equivalent for NH_3, N_2, and N_2O, while the N^{3+} and N^{4+} ion yields are dramatically weaker in the NH_3 case. Indeed, the N^{3+} ions are one order of magnitude weaker than for N_2 and N_2O and

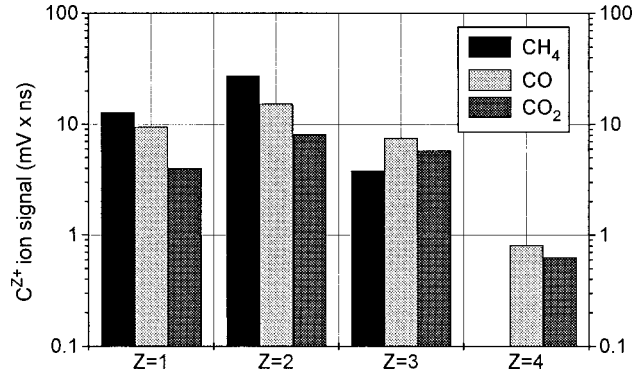

FIG. 5. Production of C^{Z+} for $Z=1-4$ from CH_4, CO, and CO_2 gases at $\lambda=800$ nm, $I=6\times10^{15}$ W/cm^2, and $p=10^{-9}$ Torr.

N^{4+} is not detected. Concerning N_2 and N_2O, the N^{Z+} ion yields are of the same order of magnitude.

B. Molecules with C atoms

The TOF spectra were recorded for CH_4, CO, and CO_2 and exhibit the same tendencies observed with molecules built with N atoms. The conclusions concerning the multicharged C^{Z+} ion peak heights and widths are quite similar to the conclusions in Sec. III A. In Fig. 5 the C^+ and C^{2+} ion yields decrease from CH_4 to CO_2. This tendency is reversed for $Z\geqslant3$ since the C^{3+} ion production is definitively less for CH_4. Moreover, no C^{4+} ion is detected in this case. In particular, the peak with the $M/Z=3$ ratio was unambiguously assigned to H_3^+ ions using different laser polarizations and intensities in comparison with the C^{Z+} $(Z=1-3)$ ion peaks. Finally, for all detected charge states up to $Z=4$, CO is more efficient than CO_2. This observation shows that the laser-molecule coupling is larger with the triple bond of CO than with the two C═O double bonds of CO_2.

Figure 6 represents the TOF spectra of CH_4, C_2H_4, and C_3H_4. The multifragmentation of the C_3 linear chain of C_3H_4 into multicharged atomic C^{Z+} ions has been studied previously in our laboratory [17]. It was shown that it is a direct process into $C^{Z+}+C^{Z'+}+C^{Z''+}$ channels with no intermediate $C_2H_n^+$ ion step. Indeed, the $C_2H_n^+$ ion peaks are very weak in Fig. 6. The three molecules C^{Z+} ion yields are compared in Fig. 7. The C^+ and C^{2+} ions production is equivalent for CH_4, C_2H_4, and C_3H_4 if we take into account the number of initial carbon atoms (1–3) within each molecule. However, for C^{3+} and C^{4+} ions, the ion yields drop for CH_4, while they exhibit approximately the same values for C_2H_4 and C_3H_4. These two molecules are built with the same C═C double bonds and exhibit the same coupling efficiency with the laser field.

C. Molecules with O atoms

For this last comparison, TOF spectra were recorded with O_2 and CO_2 and with the residual gas of the vacuum chamber at 3×10^{-10} Torr that is mainly composed of H_2O molecules and large organic molecules (Fig. 8). As in the case of carbon and nitrogen, the most striking feature of Fig. 8 is the absence of O^{3+} ions in the TOF spectrum of H_2O, while significant O^{3+} ion peaks are observed with O_2 and CO_2. The number of O^{Z+} $(Z=1-4)$ ions for O_2 and CO_2 is reported

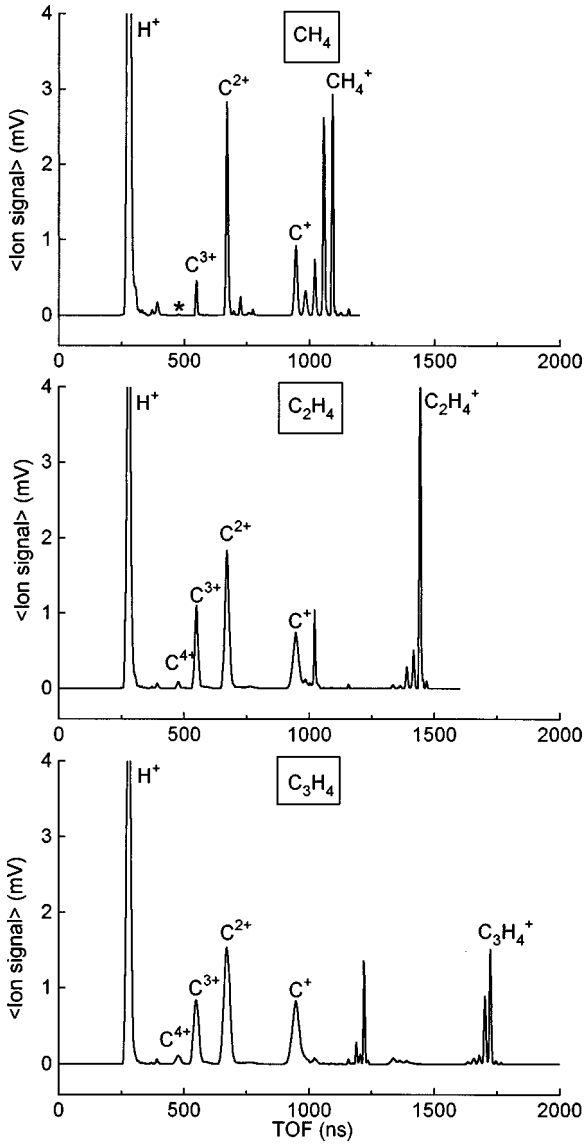

FIG. 6. Time-of-flight spectra of CH_4, C_2H_4, and C_3H_4 recorded at $\lambda=800$ nm, $I=6\times10^{15}$ W/cm^2, and $p=10^{-9}$ Torr. For CH_4, the ion peak labeled with an asterisk has been unambiguously assigned to H_3^+ ions because of the same $M/Z=3$ ratio with the C^{4+} ions.

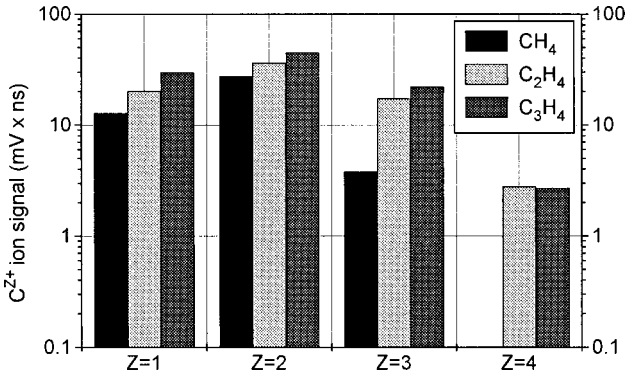

FIG. 7. Production of C^{Z+} for $Z=1-4$ from CH_4, C_2H_4, and C_3H_4 gases at $\lambda=800$ nm, $I=6\times10^{15}$ W/cm^2, and $p=10^{-9}$ Torr.

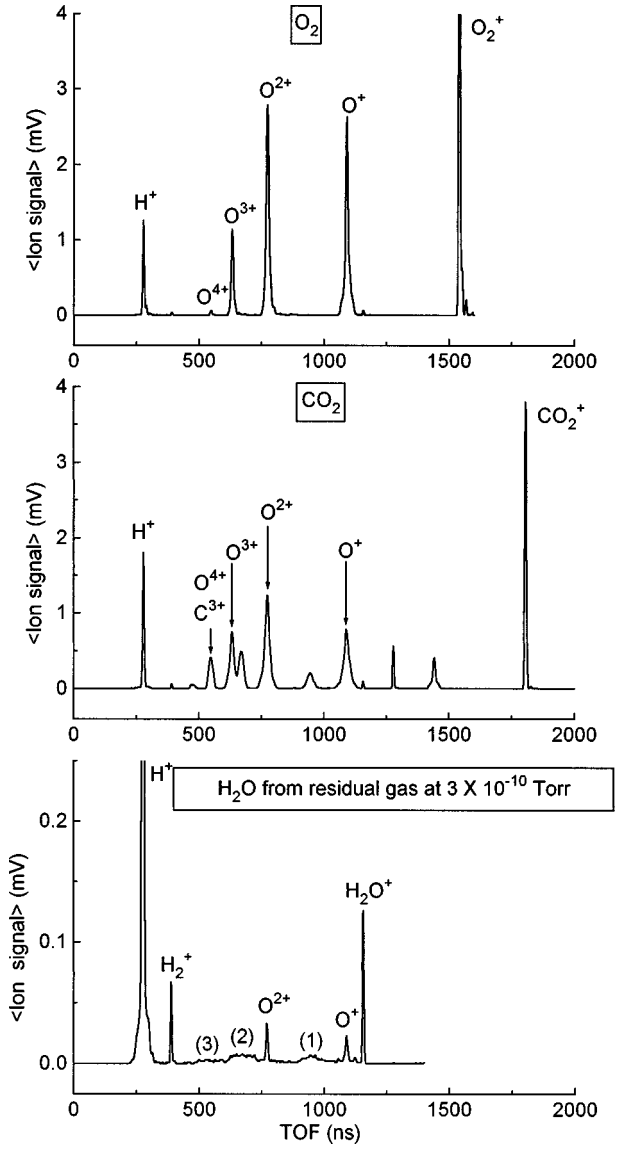

FIG. 8. Time-of-flight spectra of O_2 and CO_2 recorded at $\lambda=800$ nm, $I=6\times10^{15}$ W/cm^2, and $p=10^{-9}$ Torr. The H_2O time-of-flight spectrum has been recorded using the same laser excitation conditions but simply from the residual gas background at 3×10^{-10} Torr. In this spectrum, the ions peaks labeled (1), (2), and (3) are due to, respectively, energetic C^+, C^{2+}, and C^{3+} carbon ions coming from residual large organic molecules. These molecules enhance noticeably the proton's H^+ production.

in Fig. 9. In the case of CO_2, the C^{3+} and O^{4+} ions exhibit the same time of flight with the laser polarization direction perpendicular to the detection axis. In order to evaluate the associated ion yields, the laser electric field was set parallel to the detection axis, so that the higher kinetic energy of the O^{4+} ion allows one to separate the C^{3+} and forward and backward O^{4+} ion peaks. Both molecules exhibit ion yields with the same order of magnitude, contrary to the H_2O case.

IV. DISCUSSION

A. Comparison with field-ionization models

The field over-the-barrier ionization models give analytical expressions of the laser field required for multiple ionization. In this approach, the laser field is considered as a quasistatic field F. This implicitly assumes that the ionization time is smaller than the laser half period. In the atomic case, the model is based on the single ionization of a $A^{(Z-1)+}$ ion following

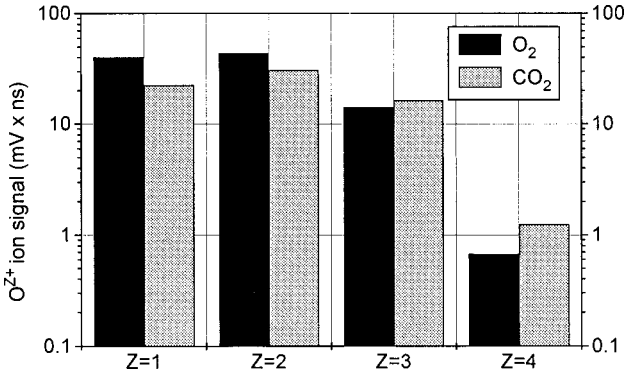

FIG. 9. Production of O^{Z+} for $Z=1-4$ from O_2 and CO_2 gases at $\lambda=800$ nm, $I=6\times10^{15}$ W/cm^2, and $p=10^{-9}$ Torr.

$$A^{(Z-1)+}+\text{laser}\rightarrow A^{Z+}+e^-. \tag{4}$$

The electronic one-dimensional potential $V_a(x)$ is the superposition of the Coulomb potential $-Z/|x|$ and the electric-dipole interaction energy $-Fx$, where x is the electron position relative to the $A^{(Z-1)+}$ core [Fig. 10(a)]. Atomic units are used throughout this section. The ionization occurs when the maximum value of $V_a(x)$ for the right barrier in Fig. 10(a) is below the ionization energy $E_{Z\leftarrow Z-1}$ of the $A^{(Z-1)+}$ ion. The required field F_a is then

$$F_a=(E_{Z\leftarrow Z-1})^2/4Z. \tag{5}$$

More sophisticated approaches known as Amosov-Delone-Krainov theories [18] take into account the electron tunneling through the right barrier [Fig. 10(a)] and are able to give the ion yield as a function of the laser field F. The calculations are in good agreement with the experimental data when the successive single ionizations dominate the direct multielectron ionizations. However, F_a remains a good estimate of the laser saturation intensity of the ion yield [2].

In the diatomic case, the model was developed by Posthumus *et al.* for the ionization of an $AB^{(Z+Z'-1)+}$ molecular ion following [8]

$$AB^{(Z+Z'-1)+}+\text{laser}\rightarrow A^{Z+}+B^{Z'+}+e^-. \tag{6}$$

Here we consider two cases to simplify the discussion. The first one is $A=B$ and $Z=Z'$ for molecules composed of identical atoms. The second one is $B=\text{H}$ and $Z'=1$ for molecules composed of an A atom and a hydrogen atom. The one-dimensional potential $V_m(x)$ experienced by the departing electron in the molecular and laser fields is

$$V_m(x)=-Z/|x-R_Z|-Z'/|x-R_{Z'}|-Fx, \tag{7}$$

where x, R_Z, and $R_{Z'}$ are the positions of, respectively, the active electron and the A^{Z+} and $B^{Z'+}$ attracting ions. $V_m(x)$ is represented in Fig. 10(b) in the case $Z'=Z$. According to the ideas developed in [8], the ionization takes place when

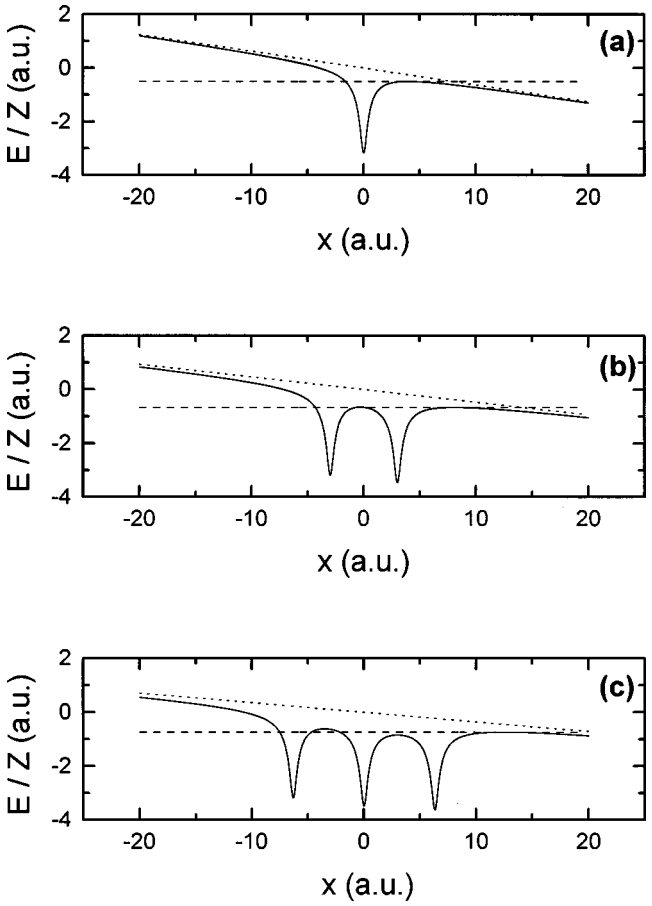

FIG. 10. Field ionization model of an electron in the combined atomic or molecular and laser fields for (a) an atomic ($A^{Z+}+e^-$) system, (b) a diatomic (A^{Z+},A^{Z+},e^-) system, and (c) a linear triatomic (A^{Z+},A^{Z+},A^{Z+},e^-) system. The full, dashed, and dotted curves represent, respectively, the electron potential energy $V_m(x)$ as a function of the electron position x (see Sec. II and Table I), the electron binding energy E_b, and the laser-electron dipolar coupling $-Fx$ in a.u.

the electron binding energy E_b is equal to the maximum of the inner barrier $V_m(x=0)$. The significance of the inner barrier touching the electron energy level is equivalent to the nonadiabatic localization of the electronic wave function in the rising well introduced by Seideman *et al.* using a full quantum calculation [9]. This condition gives the critical internuclear distance R_c for the ionization of the system [8]. The required laser field F_m for the ionization process (6) is obtained when the outer barrier maximum ($x>R_{Z'}$) is equal to the binding energy of the electron E_b.

Table I summarizes expressions for barrier tunneling model parameters. The binding energies E_b are calculated from the differences of the Coulomb potential curves of $A^{Z+}+B^{Z'}$ and $A^{(Z-1)+}+B^{Z'}$ ($E_b=-E_{Z\leftarrow Z-1}-Z'/R$). The critical distance R_c for the electron departure is always smaller in the $AH(Z,1)$ system than in the $A_2(Z,Z)$ system because of the lower attracting molecular field in the first case. Due to the fact that the ratio $Z/E_{Z\leftarrow Z-1}$ does not vary very much (1.87 for N^+, 1.84 for N^{2+}, and 1.72 for N^{3+}), the nuclear separation distance R_c for the ionization process (6) remains practically the same for different final ion charge states. Finally, the field F_m is expressed in Table I as the ratio F_m/F_a, where $F_a=(E_{Z\leftarrow Z-1})^2/4Z$ is the field necessary to ionize a bare $A^{(Z-1)+}$ ion. In the (Z,Z) case, the most striking feature is that the laser field required to produce an A^{Z+} ion from a molecule ($F_m=0.75F_a$) is weaker than the corresponding laser field F_a for an atom, although the number of removed molecular electrons is twice the number of removed atomic electrons. In the $(Z,1)$ case, the ratio F_m/F_a is given by a function $c(Z)$ reported in Table II. As Z increases from $Z=1$ to 4, the F_m field value increases from $0.75F_a$ to $1.30F_a$. Because the electron localization occurs at a shorter internuclear distance R_c, the ionization requires a higher field than in the (Z,Z) case. As a consequence, molecules built with A—H bonds will produce fewer multicharged A^{Z+} atomic ions than molecules built with A—A bonds using the same laser intensity in both cases. This statement is in good agreement with our experimental findings. In particular, for $Z=4$, the ratio of the fields for AH and A_2 is $F_m(AH)/F_m(A_2)=1.73$. Following Tables I and II, the laser intensities to produce N^{4+} ion from N, N_2, and NH are, respectively, 9.1×10^{15}, 6.8×10^{15}, and 1.2×10^{16} W/cm^2. These numbers give an explanation for the absence of N^{4+} ions at 6×10^{15} W/cm^2 in the NH_3 case.

For AH_n molecules, our results show that the multiple ionization cannot be reduced to the multiple ionization of a bare C or N atom since the AH_n^+ cation peak remains very strong in the TOF spectra. The internuclear evolutions ΔR during a half laser period $\tau_{1/2}=1.33$ fs at $\lambda=800$ nm lie in the range $10^{-2}-10^{-1}$ Å for the AH and A_2 systems where A is a C, N, or O atom. As a consequence, the proton loss is

TABLE I. Model predictions in a.u. for field ionization in the case of $A_2(Z,Z)$: $A_2^{(2Z-1)+}+\text{laser}\rightarrow A^{Z+}+A^{Z+}+e^-$ and $AH(Z,1)$: $AZ^{Z+}\rightarrow A^{Z+}+H^++e^-$. The physical quantities E_b, $V_m(x=0)$, R_c, and F_m are, respectively, the electron binding energy, the maximum value of the inner barrier, the critical internuclear distance for ionization, and the laser electric field. All these values are expressed as functions of the internuclear distance R, the charge state Z of the resulting A^{Z+} ion, the ionization potential $E_{Z\leftarrow Z-1}$ of the $A^{(Z-1)+}$ ion, and the electric field $F_a=(E_{Z\leftarrow Z-1})^2/4Z$ for the ionization of an $A^{(Z-1)+}$ atomic ion. The ratio $c(Z)=F_m/F_a$ for the $AH(Z,1)$ system is given in Table II.

Quantity	$A_2(Z,Z)$	$AH(Z,1)$
E_b	$-E_{Z\leftarrow Z-1}-Z/R$	$-E_{Z\leftarrow Z-1}-1/R$
$V_m(x=0)$	$-4Z/R$	$-(Z^{1/2}+1)^2/R$
R_c	$3Z/E_{Z\leftarrow Z-1}$	$(Z+2Z^{1/2})/E_{Z\leftarrow Z-1}$
F_m/F_a	0.75	$c(Z)$

TABLE II. Values of the ratio $c(Z)=F_m/F_a$ for the $AH(Z,1)$ system as a function of the charge state Z of the resulting A^{Z+} ion. F_m and F_a are, respectively, the electric fields in the molecular and atomic cases.

Z	$c(Z)$
1	0.75
2	0.99
3	1.17
4	1.30

negligible in the time scale of the laser period so that theories of molecular-enhanced multiple ionization remain valid for AH species. Indeed, the multiple ionization of the HI molecule was investigated at $\lambda=600$ nm ($\tau_{1/2}=1$ fs) and $I=3\times10^{15}$ W/cm^2 using a 600-fs pulse duration dye laser system [19]. Up to I^{5+} ions are detected and the Coulomb explosion exhibits the fragmentation characteristics observed with homonuclear molecules. However, the nonlinear geometries of AH_n molecules allow only a qualitative comparison with the AH model. It represents an approximation since it introduces an electronic localization closer to the A atom than in the A_2 case. Indeed, the electronic densities of CH_4 and NH_3 are narrower around the C and N atoms than, for instance, in CO or N_2.

In the triatomic case, the electronic one-dimensional potential is represented in Fig. 10(c). The inner barrier maxima do not have the same energy and the electron localization concept is more difficult to apply. In addition, the attracting potential of the precursor ion $A_3^{(3Z-1)+}$ involves one $A^{(Z-1)+}$ and two A^{Z+} atomic ions so that the electron binding energy depends on the central or terminal position of the $A^{(Z-1)+}$ ion within the molecule. As a consequence, we cannot obtain a field ionization model as precise as for diatomic molecules. Our experimental results show that no noticeable enhancement is observed in the multicharged atomic ion production from diatomic to linear triatomic molecules. This might suggest that the ionization process involves only two atoms as in the diatomic case, with the terminal third one [on the left-hand side in Fig. 10(c)] acting as a spectator.

Finally, the over-the-barrier ionization model does not take into account the tunneling possibilities of the electron through the inner and left barriers in Fig. 10 and cannot give ion yields as a function of the laser intensity. Figure 11 represents the ions yields for NH_3, N_2, and N_2O for different laser intensities. At 10^{15} W/cm^2, the N^{3+} ion yield of NH_3 is two orders of magnitude lower than the ion yields of N_2 and N_2O and no N^{2+} ions are detected for NH_3 at 2×10^{14} W/cm^2. The conclusions of Sec. III at 6×10^{15} W/cm^2 remain valid for lower charge states and laser intensities. Although this behavior can be explained by the field ionization models using the Z dependence of the physical quantities in Tables I and II, a quantitative comparison demands a theory able to give ion yields as a function of the laser field.

B. Comparison with time-dependent nonperturbative theories

Different time-dependent nonperturbative models were recently developed in the framework of the Schrödinger equation [9–11] and using the Thomas-Fermi approach [20]. To our knowledge, no theoretical works were done for the response of AH and AH_n systems to an intense laser field. Therefore, only the experimental results on diatomic and linear triatomic molecules are discussed in this section. Time-dependent quantum calculations were performed by Yu, Zuo, and Bandrauk for the H_2^+ and H_3^+ ionization rates at $\lambda=1064$ nm and $I=10^{14}$ W/cm^2 using one- and three-dimensional models [10,11]. The obtained values are in the 10^{14}-s^{-1} range and no particular enhancement is found from H_2^+ to H_3^+. Although these ion species are far from the molecules studied here, they represent models for the passage from a diatomic to a triatomic molecule. According to Yu, Zuo, and Bandrauk [10,11], the electron wave-function localization and charge resonance enhanced ionization take place between two neighboring ions of the triatomic structure. Our experimental results suggest the same behavior with AB and A_2B molecules (A,B=C,N,O) since no significant enhancements are observed in the triatomic case.

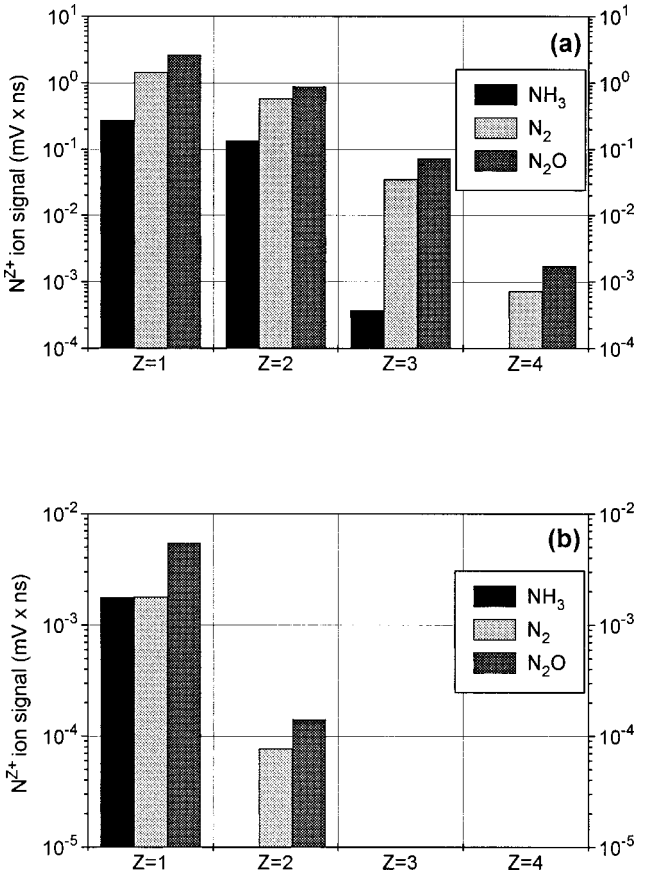

FIG. 11. Production of N^{Z+} for $Z=1-4$ from NH_3, N_2, and N_2O gases at $\lambda=800$ nm, $p=10^{-9}$ Torr, and (a) $I=10^{15}$ W/cm^2 and (b) $I=2\times10^{14}$ W/cm^2.

The Thomas-Fermi approach proposed by Brewczyk *et al.* is based on the description of the electrons as a one-dimensional charged fluid in the combined nuclear and laser fields [20]. In this case, the electronic and nuclear motions are treated on the same level using the electronic density evolution. The calculations are performed for clusters A_n with $n=2-12$ and no enhancement is predicted in the production of multicharged ions from A_2 to A_3. In conclusion, these recent models are in qualitative agreement with the experimental results. However, for quantitative comparisons, nonperturbative theories will have to include the initial three-dimensional electronic configuration.

V. CONCLUSION

In the $10^{15}-10^{16}$-W/cm^2 laser intensity range, the C^{Z+}, N^{Z+}, and O^{Z+} ($Z=1,2$) ion yields are equivalent for all the molecules studied. For $Z=3$ and 4, the AH_n molecules are definitively less efficient than the AB and linear A_2B molecules (A,B=C,N,O) and the ion yields differ by more than one order of magnitude. As a consequence, the laser-molecule coupling is more efficient for AB and A_2B

systems. This overall behavior remains basically the same at lower intensities and lower atomic charge states. For the AH_n molecules, the departing electron is mainly localized on the A^{Z+} ion and the ionization is closer to the atomic case. The AB case keeps its molecular specificity since the electron can hop from the A^{Z+} ion to the B^{Z+} ion.

The second important observation of this paper is that the multicharged ion production is equivalent for AB diatomic molecules and A_2B linear triatomic molecules with $A,B=$C,N,O, although the electronic orbitals are expected to be more delocalized in the triatomic case. The same results are obtained for the C^{Z+} $(Z=1-4)$ ions with the C_2H_4 and C_3H_4 molecules. In the framework developed for diatomic molecules by Seideman *et al.* and Yu and co-workers [9–11], the electronic wave-function localization takes place more likely between two atomic ions within the molecule with the third one acting as a spectator. However, the possible charge-exchange processes between the three wells remain to be investigated. The qualitative agreement with recent theoretical models including the Thomas-Fermi approach [20] could constitute an encouragement for the development of nonperturbative theories including an initial three-dimensional electronic configuration.

ACKNOWLEDGMENTS

The authors are pleased to acknowledge G. Vigneron (CEA/SCM) for his expertise of the kHz titanium:sapphire laser system and M. Bougeard and E. Caprin (CEA/SPAM) for their skilled technical assistance.

[1] S. Augst, D. D. Meyerhofer, D Strickland, and S. L. Chin, J. Opt. Soc. Am. B **8**, 858 (1991).
[2] T. Auguste, P. Monot, L. A. Lompré, G. Mainfray, and C. Manus, J. Phys. B **25**, 4181 (1992).
[3] B. Walker, B. Sheehy, L. F. DiMauro, P. Agostini, K. J. Schafer, and K. C. Kulander, Phys. Rev. Lett. **73**, 1227 (1994).
[4] J. B. Watson, A. Sanpera, D. G. Lappas, K. L. Knight, and K. Burnett, Phys. Rev. Lett. **78**, 1884 (1997).
[5] L. J. Frasinski, K. Codling, P. Hatherly, J. Barr, I. N. Ross, and W. T. Toner, Phys. Rev. Lett. **58**, 2424 (1987).
[6] C. Cornaggia, J. Lavancier, D. Normand, J. Morellec, P. Agostini, J.-P. Chambaret, and A. Antonetti, Phys. Rev. A **44**, 4499 (1991).
[7] C. Cornaggia, D. Normand, and J. Morellec, J. Phys. B **25**, L415 (1992).
[8] J. H. Posthumus, L. J. Frasinski, A. J. Giles, and K. Codling, J. Phys. B **28**, L349 (1995).
[9] T. Seideman, M. Yu. Ivanov, and P. B. Corkum, Phys. Rev. Lett. **75**, 2819 (1996).
[10] H. Yu, T. Zuo, and A. Bandrauk, Phys. Rev. A **54**, 3290 (1996).
[11] H. Yu and A. Bandrauk, Phys. Rev. A **56**, 685 (1997).
[12] W. C. Wiley and I. H. McLaren, Rev. Sci. Instrum. **26**, 1150 (1955).
[13] L. J. Frasinski, K. Codling, and P. A. Hatherly, Phys. Lett. A **142**, 499 (1989).
[14] C. Cornaggia, Phys. Rev. A **54**, R2555 (1996).
[15] A. Yariv, *Quantum Electronics* (Wiley, New York, 1989).
[16] Ph. Hering and C. Cornaggia (unpublished).
[17] C. Cornaggia, Phys. Rev. A **52**, R4328 (1995).
[18] M. V. Amosov, N. B. Delone, and V. P. Krainov, Zh. Eksp. Teor. Fiz. **91**, 2008 (1986) [Sov. Phys. JETP **64**, 1191 (1986)].
[19] K. Codling, L. J. Frasinski, P. Hatherly, and J. R. M. Barr, J. Phys. B **20**, L525 (1987).
[20] M. Brewczyk, C. W. Clark, M. Lewenstein, and K. Rzazewski Phys. Rev. Lett. **80**, 1857 (1998); and private communication.